Influence of initial stress distribution on liquefaction-induced settlement of shallow foundations

Bertalot, D.; Brennan, A. J.

Published in:
Geotechnique

DOI:
10.1680/geot.SIP.15.P.002

Publication date:
2015

Document Version
Publisher's PDF, also known as Version of record

Bertalot, D. & Brennan, A. J. (2015). *Géotechnique* **65**, No. 5, 418–428 [http://dx.doi.org/10.1680/geot.SIP.15.P.002]

Influence of initial stress distribution on liquefaction-induced settlement of shallow foundations

D. BERTALOT* and A. J. BRENNAN†

During earthquakes, saturated sandy soils may generate significant excess pore pressures and approach a state of liquefaction. Structures founded on shallow foundations above such soils may consequently undergo large settlements. Recent case history analysis has shown that the stress imposed by the foundation is a key factor in the estimation of such settlements. However, the case history data showed that although increasing bearing pressure caused an increase in settlements as expected, this was only true up to a point, and that very heavy structures appeared to settle less than some lighter structures. This work aims to investigate these counter-intuitive results by means of controlled experimental testing using a geotechnical centrifuge. Results of the centrifuge tests show that the trend derived from case histories is correct and that liquefaction-induced settlements peak for a given bearing stress (90 kPa for the models tested) and reduce for greater applied stresses. Further, by analysis of excess pore pressure distributions beneath the foundations it is shown that the main factor inhibiting pore pressure generation beneath the footings is not so much the confining pressure as the in-situ static shear stress around the edge of the foundation. This is supported by element test data from the literature. When this initial static shear stress is so high that the applied cyclic shear stress cannot exceed it (i.e. the direction of shear stress does not reverse) then pore pressure generation is greatly reduced, thus causing the observed reduction in expected settlements.

KEYWORDS: centrifuge modelling; footings/foundations; liquefaction

INTRODUCTION

During earthquakes, an increase in pore pressure may occur in saturated sandy/silty soils as a result of the soil structure collapse and consequent transfer of load to the pore fluid. This phenomenon results in a reduction of the effective stresses acting on the soil and a consequent degradation of the soil's shear stiffness and strength, facilitating settlement of structures having shallow foundations. If the generated excess pore pressure is high enough to induce full liquefaction underneath the footing (i.e. equals the effective overburden stress), very large deformations may take place, with one resultant phenomenon being the excessive settlement of structures with shallow foundations. A number of examples of this exist through the literature.

Data from this earthquake helped to identify an omission from the existing methods of assessing such settlements. Current practice is based primarily on the variables of footing width B and the depth of liquefiable soil D_L (Liu & Dobry, 1997). Analysis of both new and previously published case histories by Bertalot *et al.* (2013) led to the identification of footing bearing pressure q as a significant additional variable. Further, it was also identified from this analysis that, although observed settlements increased with q, this was only true for lower imposed stresses and that structures imposing stresses of the order of 100 kPa and above on the soil appeared to undergo comparatively reduced settlements. However, case history data contain significant variability in local site factors, motions and interpretation, meaning that further understanding would be better derived from controlled model testing.

Most of the current understanding of the mechanics governing soil liquefaction has been derived by laboratory element testing (mainly cyclic triaxial and cyclic simple shear tests), leading to the recognition of three main initial state variables controlling the cyclic resistance of liquefiable soils: relative density, confining pressure and static shear stress. The effect of static shear stress in particular has been the object of debate over the last 40 years, and as the stress fields beneath shallow foundations contain such static shear stresses, an understanding of this is required to capture the behaviour of such systems. Initially, cyclic triaxial tests on isotropic consolidated samples or cyclic simple shear tests on one-dimensionally consolidated samples were commonly used to assess the behaviour of saturated sands. However, despite satisfactorily reproducing the behaviour of level saturated soil deposits (where static shear stress is zero), these techniques could not capture the soil behaviour in sloping ground or underneath a footing, where significant static shear stresses are induced (Vaid & Finn, 1979). Since then, many authors have recognised that static shear stresses may, under given conditions, increase the soil's resistance to liquefaction by limiting the generation of excess pore pressure during cyclic loading (Lee & Seed, 1967; Vaid & Finn, 1979; Boulanger & Seed, 1995; Vaid *et al.*, 2001; Kammerer, 2002).

The aim of the current study is therefore to present an explanation of the apparently counter-intuitive relationship between settlement and footing bearing stress by means of a series of dynamic centrifuge tests. This will be achieved by first validating measured settlements against the case study data, then looking more closely at developed excess pore pressures, and consequently determining whether existing knowledge about static shear stresses can explain the observed pore pressures and settlement trends.

Manuscript received 27 March 2014; revised manuscript accepted 9 January 2015. Published online ahead of print 7 April 2015.
Discussion on this paper closes on 1 October 2015, for further details see p. ii.
* D'Appolonia S.p.A., Genova, Italy; also Civil Engineering Department, University of Dundee, UK.
† Civil Engineering Department, University of Dundee, UK.

CENTRIFUGE MODELLING

To achieve this aim, three centrifuge tests have been performed on the University of Dundee geotechnical centrifuge. Centrifuge modelling enables small-scale models to be tested at stress levels equivalent to a larger prototype. In this case, a length scale factor of 50 has been adopted, and a corresponding centrifugal acceleration of 50***g*** applied. All data are here reported in prototype scales; a full discussion of scaling may be found in, for example, Muir Wood (2004) or Schofield (1980). This is a 3 m diameter Actidyn C-67-2 centrifuge, equipped with the Actidyn QS-67-2 one-dimensional servo-hydraulic shaker capable of applying user-defined motions up to 0·4***g*** within the range of 0·6–8 Hz prototype scale at the 50***g*** acceleration considered (Brennan *et al.*, 2014).

Each centrifuge model tested consists of four rigid square footings ($B = 2{\cdot}75$ m at prototype scale) resting on level loose liquefiable sand ($D_R = 40\%$) deposits of different thickness. Despite having the same dimensions, each model footing exerts a different bearing pressure, namely 30, 60, 90 and 130 kPa (Figure 1). To minimise the component of the settlement due to moment-induced soil–structure interaction and resultant ratcheting of the rigid footing into the soil, footings have identical low heights and bearing pressures achieved by controlling material density (aluminium, steel and lead). All of the footing models tested are placed on the ground surface, with an embedment of 0·5 m.

All three models consist of 15 m deep deposits of clean sand with a top loose liquefiable layer ($D_R = 40\%$) and a bottom dense layer ($D_R = 80$ %). The thickness of the liquefiable layer varies in each model as the analysed tests are part of a broader testing campaign whose goal is, among others, the investigation of the role of D_L on footing settlement. The presence of the bottom dense sand layers is necessary to achieve the same overall depth of the soil deposit in the three centrifuge models. The effect of these layers was seen to have limited effects both on the overall vertical strain of the soil deposit and on the vertical propagation of the base motion. In test BD8 the top liquefiable sand layer has a depth of 8·25 m in prototype scale, whereas in test BD5 the liquefiable layer depth is reduced to 4 m measured from the foundation plan. In test BD7 the container was divided into different sectors by means of thin aluminium walls to achieve different stratification profiles

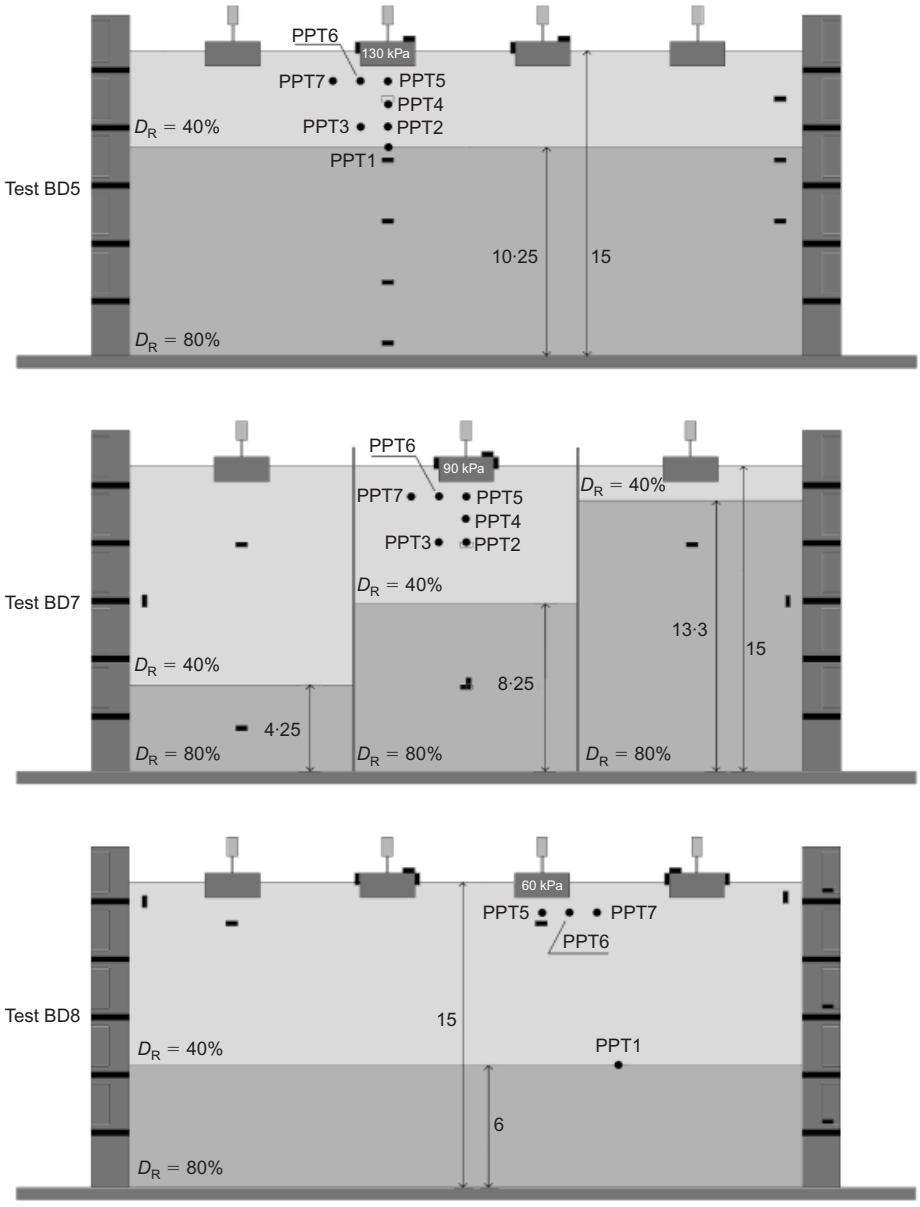

Fig. 1. Layout of centrifuge tests and instrument positions

within the same model. Thin aluminium walls (i.e. 0·3 mm thick) were used for this purpose in order to create a low lateral stiffness impermeable boundary between the different compartments, able to stop pore fluid migration without imposing constraints to the soil model. Because of the limited bending stiffness of the walls, lateral deformations at these boundaries are assumed to be controlled by the soil. In particular, liquefiable layers of 6 and 10 m have been reproduced in this test.

In order to compare the results from different tests, normalised settlements (S/D_L) are considered. This normalisation has been previously used to compare field cases of liquefaction-induced foundation settlement (Yoshimi & Tokimatsu, 1977; Liu & Dobry, 1997). Dashti *et al.* (2010) and Bertalot *et al.* (2013) pointed out that the assumption of a linear relationship between the induced settlement and liquefied soil thickness may be misleading for small B/D_L ratios. This limits the value of quantitative comparison of normalised footing settlement in different tests.

Besides footing settlement, pore pressure and acceleration are measured within the soil. In each model the pore pressure measurements were concentrated underneath a different footing, providing detailed information about the excess pore pressure generation pattern in an area with width B from the footing axis, and depth B from the foundation plan. A schematic layout of these tests is shown in Fig. 1.

The soil used for these models was HST95 Congleton silica sand; this is a fine, uniformly graded sand with rounded particle shape (Table 1). In order to achieve a correct scaling of time in both inertial and seepage controlled phenomena, a pore fluid with a viscosity 50 times higher than that of water was required (Stewart *et al.*, 1998). This was achieved by using a solution of methylcellulose in water as pore fluid, at a concentration of 2·3% of methylcellulose by mass.

Table 1. Properies of HST95 Congleton sand

Property	Measured	Lauder (2010)
G_s: g/cm^3	–	2·63
$\gamma_{d,min}$: kN/m^3	14·34	14·59
$\gamma_{d,max}$: kN/m^3	17·6	17·58
ϕ_{crit}: degrees	33	32
ϕ_{peak}: degrees*	46	44

* Indicates a property evaluated for soil at $D_R = 90\%$.

Soil models are contained in an equivalent shear beam box, consisting of stacked aluminium rings separated by thin rubber layers providing the desired flexibility (Bertalot (2012), and shown schematically in Fig. 1). The container is designed so that the shear stiffness of the end walls matches that of the soil model before soil softening due to shaking-induced excess pore pressure build-up, thereby minimising dynamic boundary effects. Upon liquefaction the soil stiffness drops significantly and this condition is no longer met; however, such stiffness reduction also inhibits the propagation of parasitic waves generating at the model boundaries due to the marked stiffness contrast.

The input motion chosen was that experienced at the primary case study site during the 2010 Maule earthquake. The initial reason is to better compare data obtained against that from the case study site (Brennan *et al.*, 2014). This motion was also seen as useful due to its long duration and large magnitude ($M_w = 8·8$), meaning that settlements achieved are likely to be an upper bound on those experienced in lower magnitude events, while also being less damaging than the sinusoidal shaking applied in older centrifuge based investigations. Fig. 2 shows the target motion record used in both time and frequency domain,

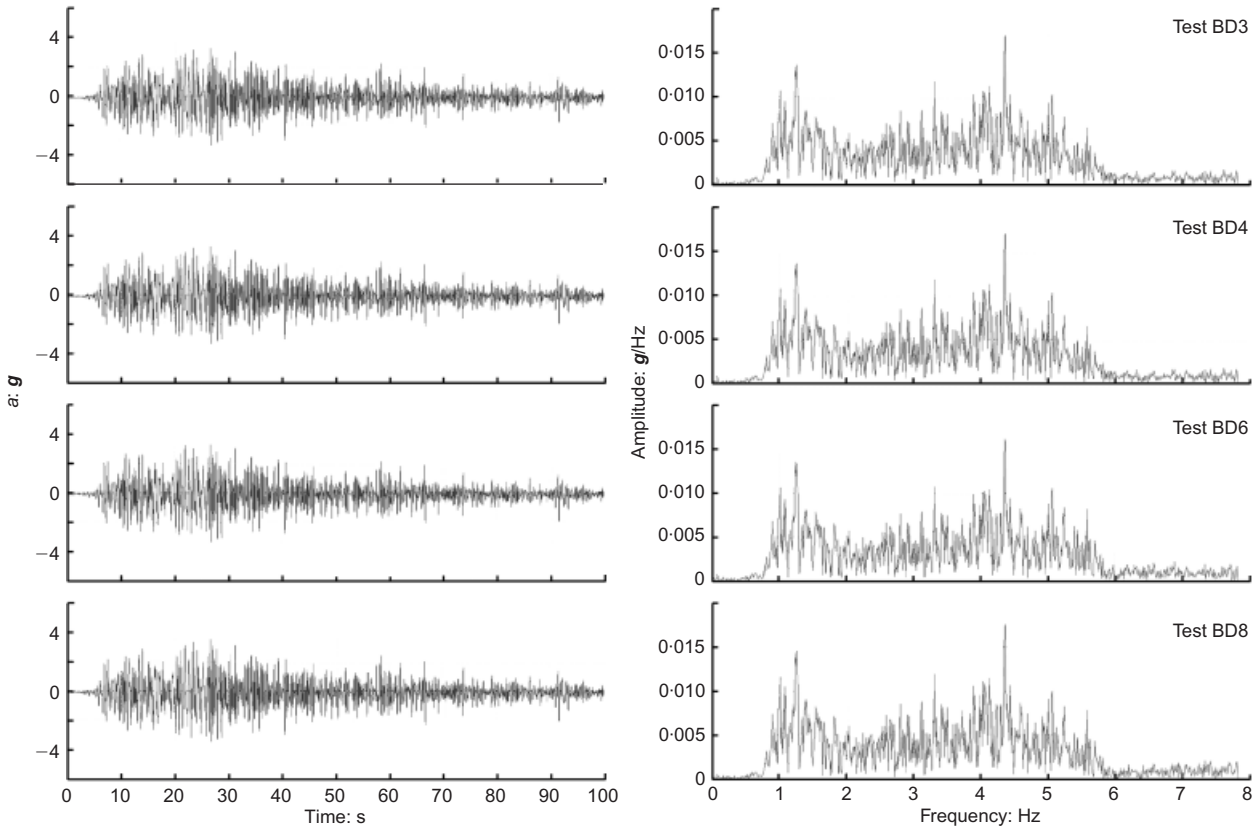

Fig. 2. Acceleration record measured at the 'Colegio Concepción' station (San Pedro de la Paz) during 2010 Maule earthquake and earthquake motions reproduced in the centrifuge tests

together with the motion recorded on the centrifuge models, indicating a very good match between target motion and achieved motion, as well as good repeatability.

SETTLEMENTS

The initial objective of this work was to validate the trend observed in field data concerning the liquefaction-induced settlement of buildings having shallow foundations. Observed settlements of such buildings from the Chile earthquake, as well as past events in Niigata (Yoshimi & Tokimatsu, 1977) and Luzon in the Philippines (Adachi *et al.*, 1992; Acacio *et al.*, 2001), are plotted as a function of bearing pressure in Fig. 3. The analysis of the documented case histories of this specific phenomenon suggests that high foundation bearing pressure may result in reduced settlement in the case of liquefaction of the foundation soil (Bertalot *et al.*, 2013). However, it is seen that there are limited field data for such heavy structures, necessitating the confirmation of this with the centrifuge models.

Figure 3 therefore also includes the total normalised settlements recorded during tests BD5, BD7 and BD8 plotted against the footing model bearing pressure. The hypothesised bearing pressure dependence of the liquefaction-induced settlement is confirmed by the experimental results. Footing settlement was indeed seen to be directly proportional to the footing's bearing pressure for bearing pressure up to about 100 kPa, as had been expected based on the field data. However, the heaviest (130 kPa) footing also experiences less settlement than the lighter ones. Data from similar experimental works from Hausler (2002) and Dashti *et al.* (2010) have also been included in Fig. 3 for comparison. In particular, Dashti *et al.* tested two types of footing models characterised by different bearing pressure (namely 76 and 120 kPa). In line with what was observed in this study, increasing the footing bearing pressure from 76 to 120 kPa did not result in further footing settlement in Dashti *et al.*'s experiment. Evidence from centrifuge test results implies that the trend identified by Bertalot *et al.* (2013) is due to a real physical phenomenon rather than arising by inconsistencies and omissions in the field data set. The remainder of this work therefore attempts to explain this trend by investigating the pore pressures beneath the footings.

EXCESS PORE PRESSURE GENERATION

The effective confining stress acting on the soil has been observed to influence its potential for excess pore pressure (Epp) generation. Steedman *et al.* (2000) performed a series of centrifuge tests investigating the cyclic behaviour of saturated sands under high confining stress (σ'_v) by testing deep level soil models with a uniform, freely draining surcharge. A reduction of the measured excess pore pressure ratio (r_u) with depth (i.e. with increasing σ'_v) was observed. Similar conditions are present beneath a footing resting on a liquefiable sand deposit. However, in this case the confining effect exerted by the footing is localised to the soil underneath it, generating a more complex stress distribution. Beside the horizontal dis-homogeneity of confining stress, shallow foundations also generate shear stresses in the foundation soil, significantly influencing its cyclic response. In order to investigate the excess pore pressure generation in such conditions, in each of the centrifuge tests performed the soil underneath one of the footing models (test BD8–60 kPa footing; test BD7–90 kPa footing; test BD5–130 kPa footing) has been instrumented with an array of pore pressure transducers (PPTs).

As instruments located at shallow depth underneath a footing are displaced proportionally to footing settlement during testing, and excess pore pressure requires reference to a measurement location, the pore pressure readings have been corrected for instrument displacement. The positions of the instruments prior to and after liquefaction were carefully measured. Correction of the excess pore pressure measurement (Epp) was then carried out by subtracting the hydrostatic surplus due to the instrument being pushed deeper into the foundation soil

$$\mathrm{Epp}(t) = \mathrm{Epp}_0(t) - (z - z_0)[S_{\mathrm{av}}(t)/S_{\mathrm{av,final}}]\gamma_w$$

where Epp_0 represents the uncorrected measurement, z and z_0 the final and initial instrument positions, respectively (below foundation plan), $S_{\mathrm{av}}(t)$ and $S_{\mathrm{av,final}}$ are the settlement at time t and the final settlement, respectively, and γ_w is the unit weight of water. It is noted that instruments did not displace laterally during testing.

Figure 4 shows the instrument initial positions and the excess pore pressure measurements during shaking from the centrifuge tests. It is acknowledged that the thickness of the liquefiable layer was different for different models.

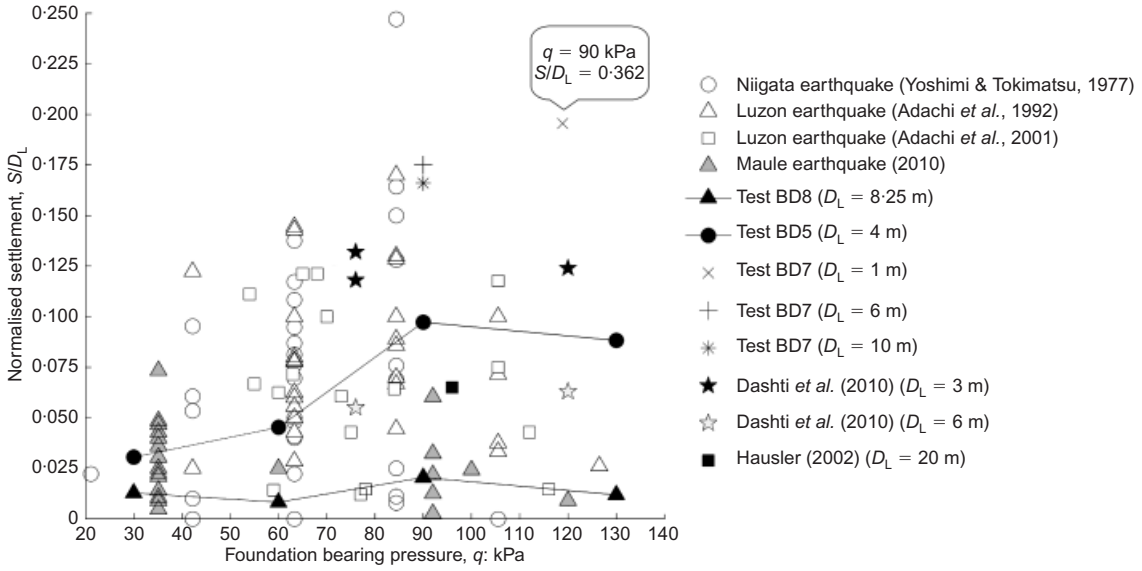

Fig. 3. Footing settlement measured in centrifuge tests BD5, BD7 and BD8 against footing bearing pressure (q)

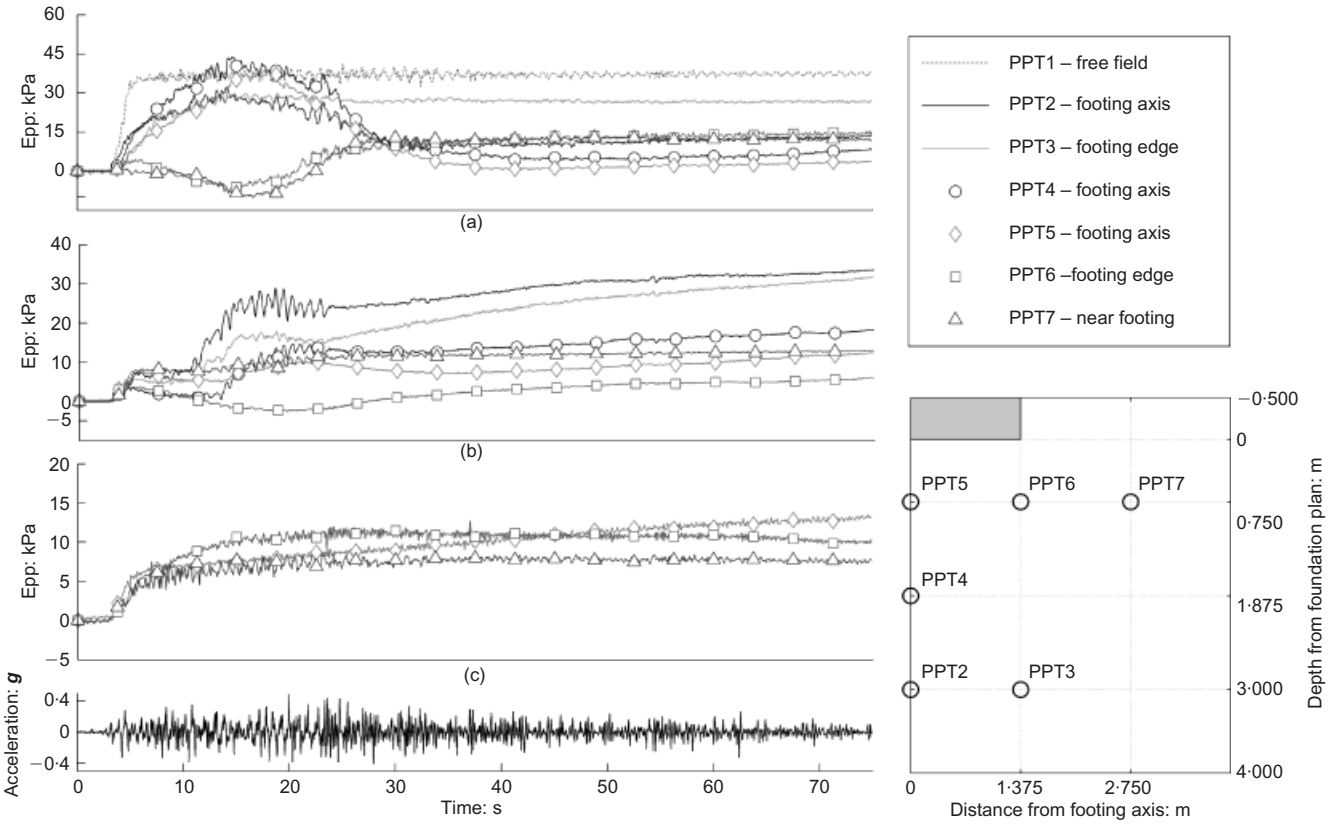

Fig. 4. During shaking Epp measurements in the soil underneath: (a) 130 kPa footing; (b) 90 kPa footing; (c) 60 kPa footing

Although this is more likely to affect the long-term pore pressure dissipation rather than the short-term pore pressure generation, there may still be variation between tests, preventing direct comparison of quantitative values. However, inspecting the distribution of pore pressures during shaking in each case is still instructive. The excess pore pressure traces in Fig. 4 show that, for the heavier footings, the lowest excess pore pressures are recorded not directly underneath the footing, but below the footing's edge. Significant positive excess pore pressures were initially generated beneath the central axis of the 130 kPa footing, while small negative excess pore pressures were recorded below the footing edge and at a distance of $B/2$ outside the footing (Figure 4(a)). Because of the pressure gradient generated as a consequence of the dis-homogeneous excess pore pressure, cross-drainage occurred during cyclic loading between different areas of the foundation soil. All of the excess pore pressures recorded show their maximum absolute value after 15 to 20 s from the start of earthquake shaking; during this time interval a maximum pressure difference of approximately 55 kPa exists between PPT5 (footing axis) and PPT7 ($B/2$ metres outside footing). As a consequence of this gradient, drainage occurs from the area below the centre of the footing towards the soil below the footing edge, leading to an equalisation of excess pore pressure in the foundation soil (after 30 s for the 130 kPa footing in Fig. 4(a)). Similar behaviour is observed underneath the 90 kPa footing; however, in this case the pressure gradients generated between the axis area and the edge area are smaller. Negative excess pore pressures were recorded only below the footing edge (PPT6), determining a less marked post-peak drainage effect (Figure 4(b)). For the lighter, 60 kPa footing, this effect seems to have been suppressed and only small differences in measured excess pore pressures are observed. In particular no negative excess pore pressures were observed below the footing edge, resulting in a fairly homogeneous excess pore pressure response across the foundation soil (Figure 4(c)).

Comparing the settlement–, acceleration– and pore pressure–time histories during shaking relative to the 130 kPa footing and the underlying soil, four main phases can be identified (Figure 5).

(*a*) Significant excess pore pressures are generated underneath the central axis of the footing, exceeding the vertical effective stress in the free-field (~12 kPa at $z = 0{\cdot}75$ m below foundation plan). On the contrary, zero or negative excess pore pressures are generated in the proximity of the footing edges. Footing settlement starts as soon as excess pore pressures are generated in the foundation soil and reaches its maximum rate during this phase.

(*b*) Significant pressure gradient exists between the axis and the edge of the footing. Cross-drainage towards the area underneath the footing edge, and possibly dilative behaviour in the foundation soil caused by the settling footing, act to reduce the excess pore pressure under the centre of the footing. During this phase the seismic loading on the soil reduces because of excess-pore-pressure-induced soil softening. During this phase, the rate of footing settlement also reduces.

(*c*) Following cross-drainage, a more homogeneous excess pore pressure distribution in the foundation soil has been reached. However, a steady and relatively slow increase in the pore pressure is observed underneath the footing. A possible explanation for this is the vertical dissipation of excess pore pressure from the underlying soil. It is hypothesised that, in the short term, fluid would migrate toward areas characterised by higher effective stresses, which can accommodate higher pore pressure with respect to the free field. Footing settlement rate further reduces during this phase, reaching its final equilibrium.

(*d*) This phase corresponds to the post-shaking behaviour. The drainage toward the foundation soil observed in phase (*c*) does not stop at the end of shaking, but rather a

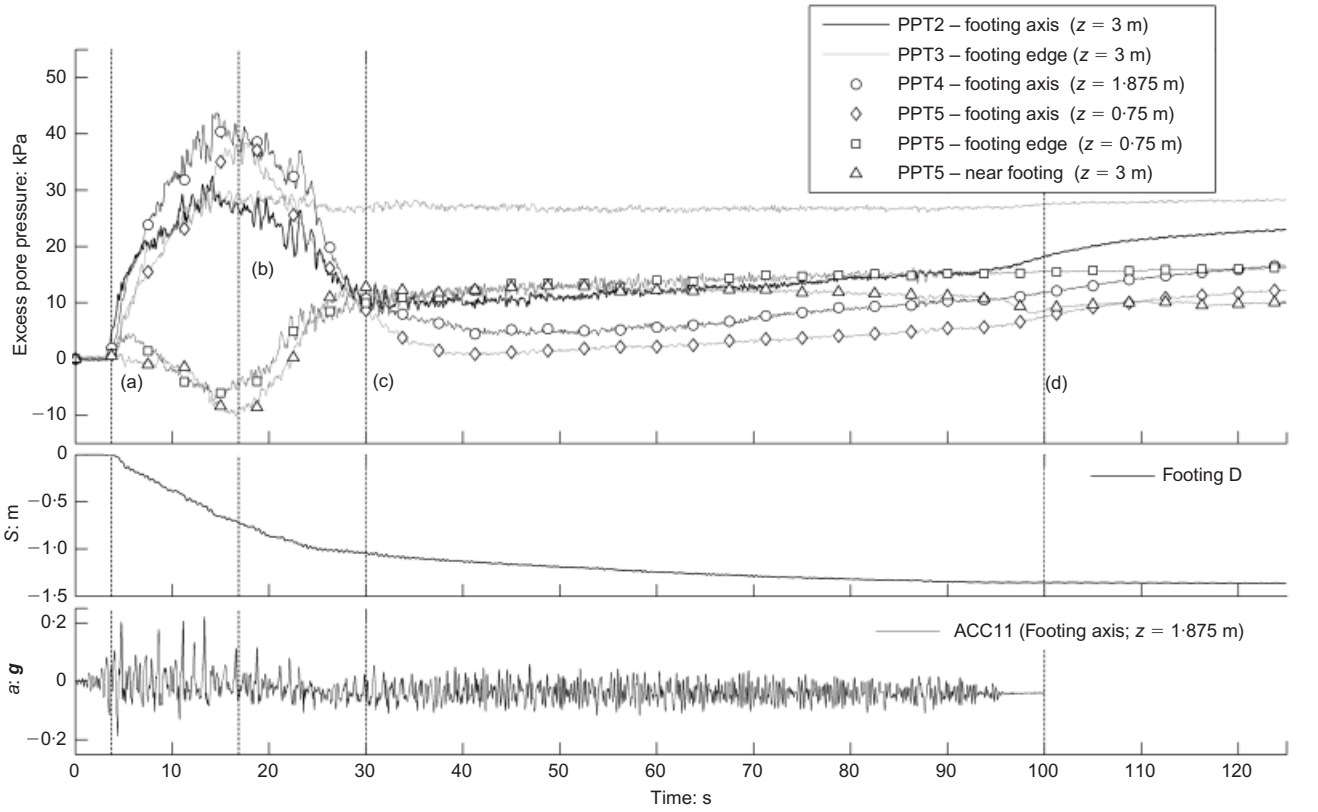

Fig. 5. During shaking Epp, settlement and horizontal acceleration measurements in the soil underneath the 130 kPa footing in test BD5

slight increase in its rate is observed, possibly due to the ceasing of the cyclic dilative response associated with the co-seismic soil behaviour. Pore pressures in the free field seem unaffected from phase (*c*). Footing settlement relative to the soil ceases with the end of shaking; however, further vertical footing displacement occurs in the longer term due to the dissipation of excess pore pressure associated with the post-liquefaction reconsolidation of sands (i.e. volumetric settlement).

These data therefore show that the main cause for limiting excess pore pressure generation is associated with the soil beneath the edge of the footing. As this is where initial static shear stresses are at a maximum, and as static shear stresses have previously been identified with increased cyclic resistance under certain conditions, their potential correlation with these results is examined further in the next section. This mechanism has not been previously identified in similar works (Whitman & Lambe, 1982; Liu & Dobry, 1997; Hausler, 2002; Dashti *et al.*, 2010) as the instrument distribution was not targeted to pick up variations in pore pressure within the space beneath the foundations.

INFLUENCE OF INITIAL SHEAR STRESS

The effect of static shear stress on the cyclic resistance to liquefaction has been investigated by several authors since the late 1960s. Most of the experimental work on this topic is based on soil element testing, in particular cyclic triaxial testing. Lee & Seed (1967) first hypothesised that the presence of static shear increases the soil's cyclic resistance to liquefaction by performing a series of cyclic triaxial tests on anisotropically consolidated samples. Subsequently, Castro (1969, 1975) and Castro & Poulos (1977) verified that the presence of static shear may result in a reduction of the cyclic resistance of sand. These apparently contradictory results were unified in a more complex framework by Vaid & Finn (1979) and Vaid & Chern (1983, 1985), who showed the effect of static shear to be strongly dependent on the initial confining stress and soil density. The results of these studies show that the initial state variables considered (static shear, confining stress, relative density) control the cyclic behaviour of saturated sands, and that their effects are mutually dependent. The soil relative density in particular will determine the mechanism of strain development, strain softening taking place in loose and strongly contractive soils and 'cyclic mobility' (or limited strain liquefaction) in denser soils (Castro, 1975). Again, the threshold density between these two mechanisms, other than on the soil type, depends on the confining stress and static shear acting on the soil.

The addition of an initial shear stress in loose contractive materials would therefore lower its resistance to liquefaction as it moves it closer to the failure envelope. However, if such initial shear stress (τ_i) is higher than the cyclic shear stresses (τ_{cyc}) applied, than no stress reversal takes place in the soil, significantly increasing its cyclic resistance (Vaid & Finn, 1979; Boulanger & Seed, 1995; Kammerer, 2002).

In order to adapt the empirical liquefaction triggering curves used in current practice, which are based on level ground conditions case histories, to sloping ground conditions (i.e. presence of static shear), Seed (1983) first proposed a correction factor K_α dependent on the static shear. Several sets of curves relating K_α values to static shear stress ratio ($\alpha = \tau_i/\sigma'_v$) have subsequently been published (Seed & Harder, 1990; Harder & Boulanger, 1997).

Similarly, an independent factor (K_σ) is used in current practice to account for the influence of confining stress on the soil liquefaction resistance. Based on the collective dependency of cyclic resistance on all initial state variables, Vaid *et al.* (2001) question the use of independent factors in order to account for confining stress and static shear. Results of a series of cyclic triaxial tests on Fraser River sand, presented by the authors, show that the empirical method

currently used underestimates the cyclic resistance, the degree of conservatism being more dramatic for loose soils (Fig. 6).

Effect of initial shear stress in the centrifuge tests

Despite significant differences between the loading and boundary conditions of an element test and those of an element of soil in a centrifuge model (or in the field), these findings can still be used to inform interpretation of the soil behaviour observed in the centrifuge tests. One of the main differences in soil behaviour is that element tests are usually performed in fully undrained conditions, while results show that partially drained conditions apply to centrifuge tests (Madabhushi & Haigh, 2012; Lakeland *et al.*, 2014). Stress distribution in the two cases may also vary significantly. In particular, in cyclic triaxial tests the soil is subjected to different admissible soil deformations and the total stress is kept constant, while in centrifuge tests it may vary during cyclic loading.

The effect of static shear stresses on the cyclic response of the soil depends on the ranges of state variables represented in the centrifuge tests (σ'_v varying between approximately 30 and 160 kPa between foundation plan and a depth equal to B metres below foundation plan; and $D_R = 40\%$). According to the K_α values proposed by Seed & Harder (1990), the presence of the footing-induced static shear stress within these ranges of state variables should result in a reduction of the foundation soil's cyclic resistance (Fig. 6). On the contrary, in the centrifuge tests performed, reduced excess pore pressure generation was observed in soil associated with high static shear stresses (i.e. increased cyclic resistance). This is in accordance with the K_α curves proposed by Vaid *et al.* (2001) for relative density of 40% and a similar initial confining stress. Results from Vaid *et al.* (2001) may be considered more reliable as, unlike the Seed & Harder (1990) formulation, they account for the combined effect of confining stress and relative density.

In order to identify the initial distribution of static shear stress present in the centrifuge model, the contours of α along a longitudinal section of the model have been computed based on a finite-element simulation performed using the software Plaxis2D. The built-in elastic perfectly-plastic Mohr–Coulomb material model was used for this purpose.

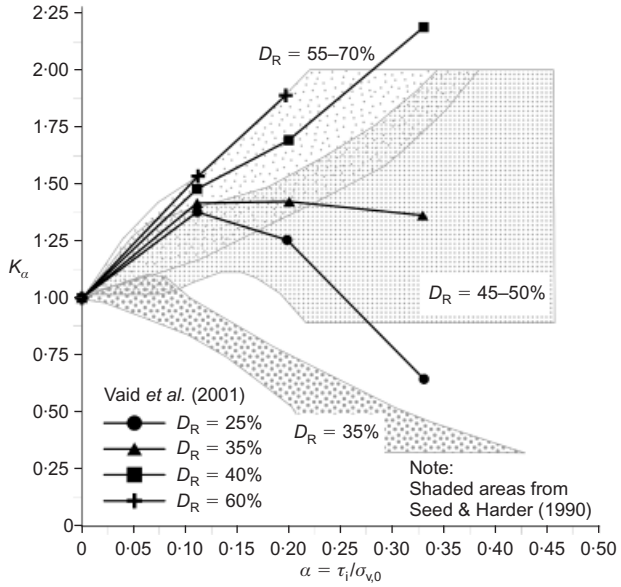

Fig. 6. K_α plotted against α for Fraser River sand at different density states and σ'_v of 100 kPa (Vaid *et al.*, 2001)

The mechanical parameters required by the model are shown in Table 2. The computed stress distribution describes the static case before earthquake shaking, and is shown in Fig. 7 (to the right of the axis of each footing in the figure). During shaking the soil–structure interaction may result in a different, time-dependent, distribution of such stresses, reflecting the foundation tendency to rock and translate horizontally, and thus cyclically extending both laterally and downward. Therefore, the computed stress distribution has to be considered only indicative. The typical α distribution induced by a shallow foundation consists of 'bulbs' of high α beneath the footing edges, the extension of such bulbs being proportional to the foundation bearing pressure.

Also plotted on Fig. 7 (to the left of the axis of each footing in the figure) are contours of the peak excess pore pressure before drainage, measured in the foundation soil below the 60, 90 and 130 kPa footings, respectively. Contours are obtained by interpolating between data points using a linear interpolation scheme. Contours are plotted such that darker colours represent lower pore pressures.

Comparison between excess pore pressures and static shear stresses in Fig. 7 shows that the observed reduction in the generated excess pore pressure below the footing edge corresponds, as suggested above, with areas characterised by high values of α. In particular, the minimum excess pore pressures were recorded in portions of the foundation soil characterised by $\alpha > 0{\cdot}4$ (Figs 7(a) and 7(b)). The heavier footing ($q = 130$ kPa) generates significant shear stresses in a broad portion of the foundation soil. The 'bulb' of soil characterised by a value of α higher than 0·4 extends to a depth of $\sim B$ (footing width) and has a maximum width of $\sim B/2$ (Fig. 7(a)). Pore pressure measurements in correspondence with this area show no generated excess pore pressures. On the contrary, small negative peak excess pore pressures have been recorded by PPT6 (footing edge) and PPT7 (near footing), possibly due to dilation induced by the footing settlement. Similar observations have been made for the 90 kPa footing; in this case, only records from PPT6 (footing edge) show near-zero excess pore pressure, while significant excess pore pressure was measured by PPT7, in line with those recorded at the same depth in correspondence with the footing axis (Fig. 4). A possible explanation for these observations may be that the bulb of soil with $\alpha > 0{\cdot}4$ induced by the 90 kPa footing is smaller; as a consequence the soil near PPT7 is subjected to lower shear stresses, resulting in lower cyclic resistance (Fig. 7(b)).

Excess pore pressures generated at a depth of 0·75 m underneath the lighter footing analysed ($q = 60$ kPa) show little or no horizontal variability from the footing axis to a distance of $B/2$ from the footing edge (Fig. 7(c)). In particular, the excess pore pressure generation pattern observed is similar to what is observed in the free-field case (i.e. $\tau_i = 0$), suggesting a reduced influence of the footing-induced stresses for lower bearing pressure.

In all cases the highest excess pore pressure values were recorded beneath the footing axis, where the shear stresses are a minimum. Despite full liquefaction (i.e. $r_u = 100$ %) being observed in the free field in all of the models tested,

Table 2. Plaxis 2D linear-elastic perfectly-plastic Mohr–Coulomb model parameters (HST95 Congleton sand at $D_R = 40\%$)

E: MPa	25
υ	0·3
γ_d: kN/m^3	15·49
ϕ_{crit}: degrees	33
ψ: degrees*	1

* Measured at $D_R = 40\%$.

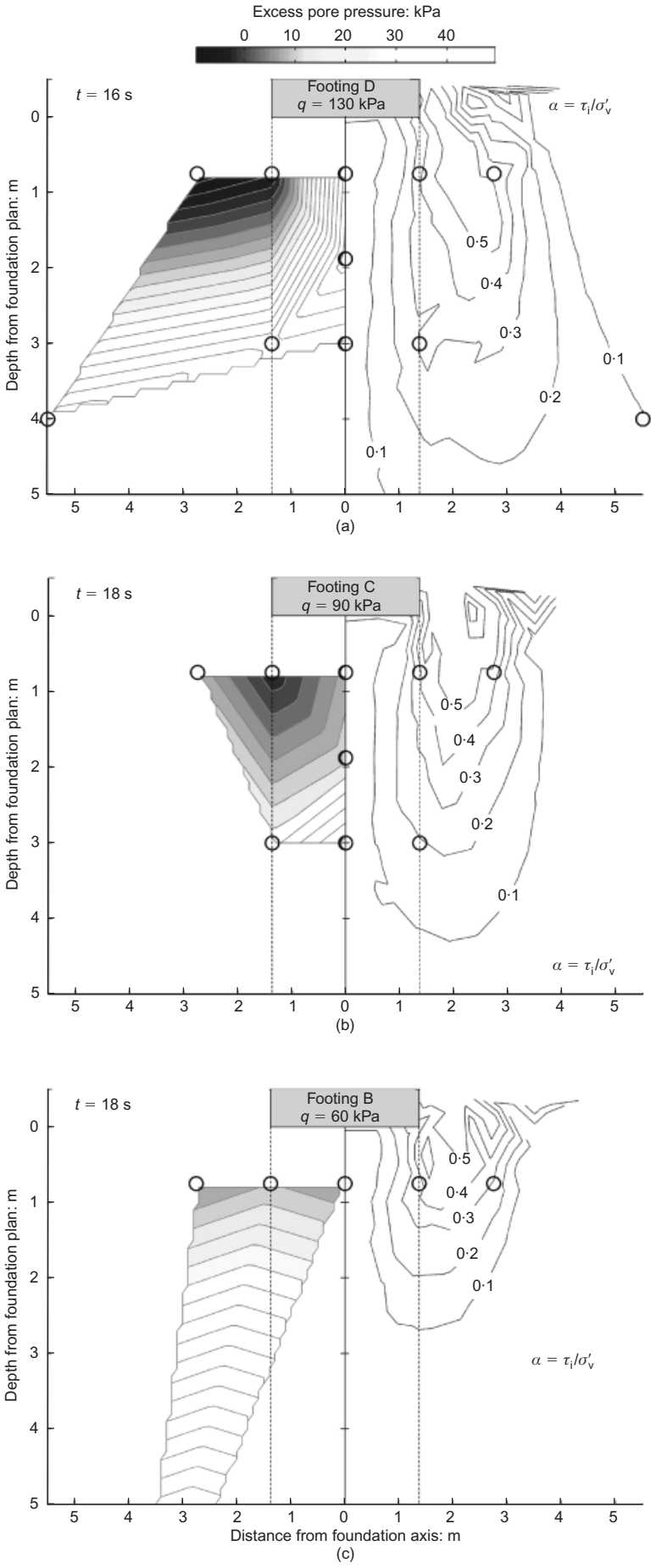

Fig. 7. Contours of peak Epp before drainage against contours of footing-induced static shear stress ratios: (a) 130 kPa footing; (b) 90 kPa footing; (c) 60 kPa footing

all the PPTs positioned in the soil below or in the proximity of the footings recorded peak excess pore pressure ratios ($r_{u,max} = Epp_{max}/\sigma'_v$) significantly lower than 100%. This is plotted in Fig. 8, which shows the $r_{u,max}$ recorded beneath the footings against the estimated initial shear stress ratio at the measurement location. Also in Fig. 8, the results from the centrifuge tests are compared to those from cyclic shear tests performed by Kammerer (2002) and Boulanger *et al.* (1991) for different values of α. For higher α, all three sets of data show a decrease of the recorded excess pore pressure ratio for increasing initial static shear stress ratio. However, a substantial difference exists between centrifuge and cyclic shear data for low values of initial static shear stress ratio, which is ascribed to the different boundary conditions. Theoretically, applying horizontal fixity and no-flow boundary conditions to the soil column below the footing, if liquefaction is triggered the entire weight of the footing would be transferred to the pore fluid, reaching a state of full liquefaction. These idealised boundary conditions are unrepresentative of reality where significant cross-drainage occurs during shaking, resulting in peak r_u values lower than unity.

A threshold value of α exists, above which excess pore pressure generation is impeded. Such a threshold value is not unique but depends, other than soil type, on relative density and confining stress. For the range of confining stress and relative density considered in the models tested, α values higher than ~0·4 showed zero or negative excess pore pressure generation. Results from a series of cyclic bi-directional simple shear tests performed by Kammerer (2002) on Monterey #0/30 sand show a similar threshold value (Fig. 8).

These observations suggest that, in all of the analysed cases, the foundation soil underwent excess pore pressure-induced softening without reaching a condition of full liquefaction (i.e. $r_u = 100\%$). Moreover, in the presence of significant static shear stress, areas of non-softened soil may initially exist below the edges of the footing during earthquake shaking, even in the case where the motion is strong enough to trigger liquefaction in the free field.

Effect of shear stress reversal

As mentioned above, many authors have stressed the influence of shear stress reversal on cyclic excess pore pressure generation (Vaid & Finn, 1979; Boulanger & Seed, 1995; Kammerer, 2002). Shear stress reversal occurs when the oscillating earthquake-induced shear stress (τ_{cyc}) exceeds the static shear stress (τ_i), crossing a state of zero shear and thus reversing direction. However, the magnitude of τ_i and τ_{cyc} is not sufficient information to evaluate the degree of stress reversal, as the direction of such stresses has to be taken into consideration as well. Kammerer (2002) points out that, in the case of sloping ground, τ_i will be oriented parallel to the dip direction of the slope, while the direction of τ_{cyc} is variable depending on the ground motion. In this scenario, the potential for stress reversal is higher when the principal direction of seismic loading is parallel to the dip direction of a slope. However, the author observes that significant excess pore pressures are generated in the soil even when the direction of loading is parallel to the strike direction of the slope. This is ascribed to the correspondent complementary shear stresses acting perpendicularly to the loading direction. Unlike those generated in slopes, the direction of the maximum shear stresses induced by a footing in the foundation soil changes with depth. This increases the complexity in the evaluation of the effect of shear stress reversal on the excess pore pressure generation below shallow foundations.

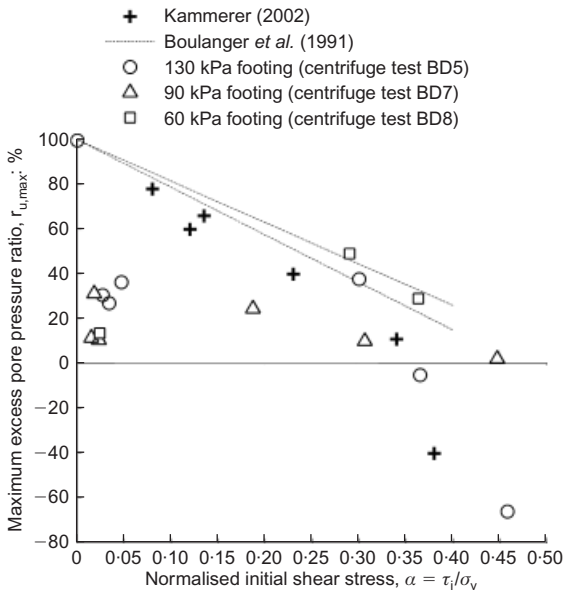

Fig. 8. α values at Epp measurement point against $r_{u,max}$ together with data from bi-directional direct shear tests from Kammerer (2002) and Boulanger *et al.* (1991)

Figure 9 compares the estimated stress paths in two soil elements located at the same depth below the foundation plan ($z = 0{\cdot}75$ m), the first corresponding to the central axis of the 130 kPa footing (PPT5) and the second beneath the footing edge (PPT6). Since no stress measurement is available at the selected locations, the proposed stress paths represent an estimate based on the following assumptions.

(*a*) The initial static shear stress (from static finite-element simulation) is assumed to be maintained during the entire earthquake.
(*b*) Total vertical stress variations in the soil during earthquake shaking ($\Delta\sigma_v$) are accounted for based on the measured vertical footing accelerations. A vertical 'piston-like' footing movement is assumed and total vertical stress variations in the soil calculated according to Newton's law and Boussinesq theory.
(*c*) The static (τ_i) and cyclic (τ_{cyc}) shear stresses are assumed to act on the same plane (condition yielding maximum expected amount of shear stress reversal).

The proposed linear failure envelope (Fig. 9) corresponds to a friction angle of ~32° (Lauder, 2010), yielding a critical α value of 0·61. Under these premises, the stresses in a soil element at the selected locations can be estimated according to

$$\Delta\sigma_v(t) = B_q\,\Delta q(t) = B_q\frac{[M_f\,a_v(t)]}{A_f}$$

$$\sigma'_v(t) = \sigma'_{v,0}(t) + \Delta\sigma_v(t) - Epp$$

$$\tau_{cyc}(t) = a_h(t)\,r_d\,[\sigma'_v(t) + Epp(t)]$$

$$\tau(t) = \tau_i + \tau_{cyc}(t)$$

where B_q represents the ratio $\Delta\sigma_v/\Delta q$ evaluated at the selected locations according to Boussinesq theory, Δq is the variation in footing bearing pressure due to the footing vertical acceleration, a_v. a_h is the horizontal acceleration measured in the ground at 0·75 m below the foundation plane and r_d is a stress reduction factor evaluated according to the formulation of Idriss & Boulanger (2004).

According to the computed stress paths, no stress reversal occurs below the footing edge, whereas beneath the footing axis shear stress reverses direction in most of the loading cycles. It is also worthwhile to notice that the magnitude of the cyclic shear stress imposed to the foundation soil depends on the acting

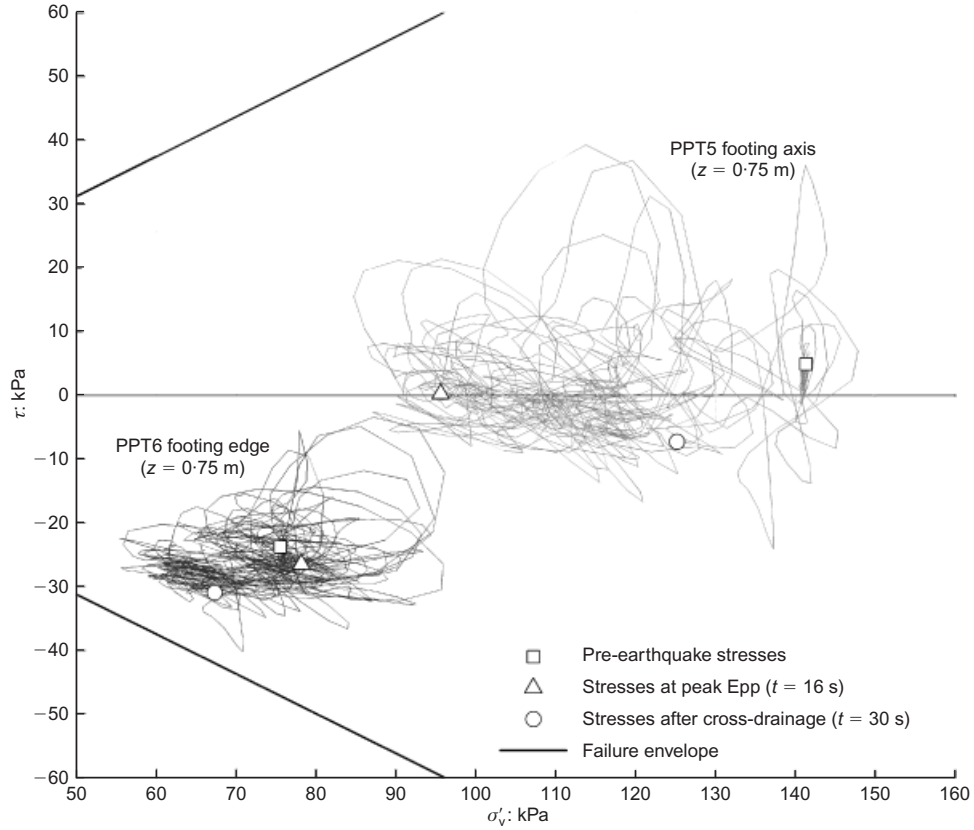

Fig. 9. Approximate stress paths in the τ–σ'_v plane, occurring during shaking beneath the footing's central axis (PPT5) and below the footing edge (PP6) (see Fig. 5(a))

vertical effective stress; therefore it is higher below the centre of the footing where σ'_v is maximum.

High τ_i brings the soil's stress state closer to failure, but at the same time reduces its potential for softening as a consequence of excess pore pressure generation. The stress path corresponding to PPT6, despite starting closer to the failure envelope than PPT5, shows no initial softening as excess pore pressure generation is impeded. Instead a slight hardening behaviour is initially observed, possibly due to dilation occurring in the soil and consequent development of negative excess pore pressure, increasing the σ'_v. However, significant softening occurs following cross-drainage, bringing the soil state closer to failure (Fig. 9). On the contrary, PPT5 shows significant softening taking place from the first cycles, reducing the acting σ'_v of about 35%. Cross-drainage in this case takes place from the footing axis toward the areas below the edge of the footing, resulting in a reduction in excess pore pressure and hence in a regain of σ'_v (Fig. 8).

CONCLUSIONS

Excess pore pressure measurements from a series of three centrifuge tests showed that, in the presence of a footing resting directly on liquefiable soil, limited or no softening occurred in the soil below the footing edge during earthquake shaking. In particular, these observations were seen to be valid for footings exerting a relatively high bearing pressure (i.e. $> \sim 100$ kPa) on the soil. Areas of the foundation soil which experienced least pore pressure increase were seen to correspond with those where the footing-induced initial shear stresses τ_i are a maximum. Partially drained loading conditions were observed in all of the centrifuge tests performed, with significant drainage taking place during shaking to equalise the initial inhomogeneous excess pore pressure generation. The comparison of the approximate stress paths between soil beneath the footing's central axis and below the footing edge suggests that the absence of shear stress reversal when initial shear stress is greater than cyclic shear stress (verified if $\tau_i > \tau_{cyc}$) may provide an explanation to the limited excess pore pressure generation observed below the edges of the footing.

These results clarify the hypothesis derived previously from case study data that, although increasing the bearing pressure of shallow foundations on liquefiable soil causes an increase in likely settlement, this is only true up to a certain stress level (here ~ 100 kPa), above which settlements may no longer increase and may even reduce. It appears from the testing performed that this is attributable to the initial shear stresses in the soil inhibiting pore pressure generation, apparently through a lack of shear stress reversal. Moreover, the soil tendency to dilate at high stress ratio may also contribute to inhibiting pore pressure generation.

The generality of the observed behaviour would be further tested by consideration of very wide footings, where the areas of high initial shear stress are proportionally less than the more uniformly loaded soil beneath the footing, and also by consideration of a wider range of input motions to investigate the relationship between τ_i and τ_{cyc}, and whether this affects the bearing pressure at which peak settlement occurs.

NOTATION

a_h	horizontal acceleration measured in ground at 0·75 m below foundation plane
a_{max}	peak ground acceleration ($\boldsymbol{g}$)
a_v	footing vertical acceleration
B	building width (m)
B_q	ratio $\Delta\sigma_v/\Delta q$ evaluated at selected locations according to Boussinesq theory
D_L	liquefied soil thickness (m)
D_R	relative density (%)

E Young's modulus (MPa)
Epp excess pore pressure (kPa)
$\text{Epp}_{\max}$ peak excess pore pressure before cross-drainage (kPa)
Epp_0 uncorrected excess pore pressure (kPa)
K_α static shear correction factor
K_σ overburden correction factor
q foundation bearing pressure (kPa)
r_d stress reduction factor evaluated according to formulation of Idriss & Boulanger (2004)
r_u excess pore pressure ratio, $\text{Epp}/\sigma'_\text{v}$ (%)
$r_{\text{u,max}}$ peak excess pore pressure ratio before cross-drainage, $\text{Epp}_{\max}/\sigma'_{\text{v},0}$ (%)
S_av average liquefaction induced settlement (m)
$S_\text{av}(t)$ settlement at time t
$S_{\text{av,final}}$ final settlement
ν Poisson ratio
z depth from foundation plane (m)
z_0 initial instrument depth (m)
α static shear stress ratio (or normalised initial shear stress), $\tau_\text{i}/\sigma'_{\text{v},0}$
γ_d dry unit weight (kN/m^3)
γ_w unit weight of water
Δq variation in footing bearing pressure due to footing vertical acceleration, a_v
σ'_v vertical effective stress (kPa)
$\sigma'_{\text{v},0}$ initial vertical effective stress (kPa)
τ_cyc cyclic shear stress (kPa)
τ_i initial (or static) shear stress (kPa)
τ_{xz} shear stress acting on the x–z plane ($\tau_\text{i} + \tau_\text{cyc}$) (kPa)
ϕ_crit friction angle at critical state (degrees)
ϕ_P peak friction angle (degrees)
ϕ_R residual friction angle (degrees)
ψ dilation angle (degrees)

REFERENCES

Acacio, A., Kobayashi, Y., Towhata, I., Bautista, R. T. & Ishihara, K. (2001). Subsidence of building foundation resting upon liquefied subsoil: case studies and assessment. *Soils Found.* **41**, No. 6, 111–128.

Adachi, T., Iwai, S., Yasui, M. & Sato, Y. (1992). Settlement and inclination of reinforced-concrete buildings in Dagupan-City due to liquefaction during the 1990 Philippine earthquake. *Proceedings of the 10th world conference on earthquake engineering*, vol. 1, pp. 147–152. Rotterdam, the Netherlands: Balkema.

Bertalot, D. (2012). *Behaviour of shallow foundations on layered soil deposits containing loose saturated sands during earthquakes*. PhD thesis, University of Dundee, UK.

Bertalot, D., Brennan, A. J. & Villalobos, F. (2013). Influence of bearing pressure on liquefaction-induced settlement of shallow foundations. *Géotechnique* **63**, No. 5, 391–399, http://dx.doi.org/10·1680/geot.11.P.040.

Boulanger, R. W. & Seed, R. B. (1995). Liquefaction of sand under bi-directional monotonic and cyclic loading. *J. Geotech. Engng, ASCE* **121**, No. 12, 870–878.

Boulanger, R. W., Seed, R. B., Chan, C. K., Seed, H. B. & Sousa, J. (1991). *Liquefaction behaviour of saturated sands under unidirectional and bi-directional monotonic and cyclic simple shear loading*, Geotechnical Engineering Report No. UCB/GT/91-08. Berkeley, CA, USA: University of California.

Brennan, A. J., Knappett, J. A., Bertalot, D., Loli, M., Anastasopoulos, I. & Brown, M. J. (2014). Dynamic centrifuge modelling facilities at the University of Dundee and their application to studying seismic case histories. In *ICPMG2014 – physical modelling in geotechnics* (eds C. Gaudin and D. White), pp. 227–234. Boca Raton, FL, USA: CRC Press.

Castro, G. (1969). *Liquefaction of sands*. PhD thesis, Harvard University, Cambridge, MA, USA.

Castro, G. (1975). Liquefaction and cyclic mobility of saturated sands. *J. Geotech. Engng, ASCE* **101**, No. 6, 551–569.

Castro, G. & Poulos, S. J. (1977). Factors affecting liquefaction and cyclic mobility. *J. Geotech. Engng Div., ASCE* **103**, No. GT6, 501–516.

Dashti, S., Bray, J. D., Pestana, J. M., Riemer, M. & Wilson, D. (2010). Mechanism of seismically induced settlement of buildings with shallow foundation on liquefiable soil. *J. Geotech. Geoenviron. Engng, ASCE* **136**, No. 1, 151–164.

Harder, L. F. Jr & Boulanger, R. W. (1997). Application of Kσ and Kα correction factors. *Proceedings of the NCEER workshop on evaluation of liquefaction resistance of soils*, report NCEER-97-0022, pp. 167-190. Buffalo, NY, USA: National Center for Earthquake Engineering Research, State University of New York.

Hausler, E. A. (2002). *Influence of ground improvement on settlement and liquefaction: a study based on field case history evidence and dynamic geotechnical centrifuge tests*. PhD thesis, University of California, Berkeley, CA, USA.

Idriss, I. M. & Boulanger, R. W. (2004). Semi empirical procedures for evaluating liquefaction potential during earthquakes. In *Proceedings of the 11th international conference on soil dynamics and earthquake engineering, and 3rd international conference on earthquake geotechnical engineering* (eds D. Doolin, A. Kammerer, T. Nogami, R. B. Seed and I. Towhata), pp. 33–56. Singapore: Stallion Press.

Kammerer, A. M. (2002). *Undrained response of Monterrey 0/30 sand under multidirectional cyclic simple shear loading conditions*. PhD thesis, University of California, Berkeley, CA, USA.

Lakeland, D. L., Rechenmacher, A. & Ghanem, R. (2014). Towards a complete model of soil liquefaction: the importance of fluid flow and grain motion. *Proc. A, R. Soc.* **470**, No. 2165, 20130453, http://dx.doi.org/10·1098/rspa.2013·0453.

Lauder, K. D. (2010). *The performance of pipeline ploughs*. PhD thesis, University of Dundee, UK.

Lee, K. L. & Seed, H. B. (1967). Dynamic strength of anisotropically consolidated sand. *J. Soil Mech. Found. Div., ASCE* **93**, No. SM5, 169–190.

Liu, L. & Dobry, R. (1997). Seismic response of shallow foundation on liquefiable sand. *J. Geotech. Geoenviron. Engng, ASCE* **123**, No. 6, 557–567.

Madabhushi, S. P. G. & Haigh, S. K. (2012). How well do we understand liquefaction. *Indian Geotech. J.* **42**, No. 3, 150–160.

Muir Wood, D. (2004). *Geotechnical modelling*. London, UK: Spon Press, Taylor and Francis.

Schofield, A. N. (1980). Cambridge geotechnical centrifuge operations. *Géotechnique* **30**, No. 3, 227–268, http://dx.doi.org/10·1680/geot.1980·30·3·227.

Seed, H. B. (1983). Earthquake resistant design of dams. In *Seismic design of embankments and caverns* (ed. T. R. Howard), pp. 41–64. New York, NY, USA: American Society of Civil Engineers.

Seed, R. B. & Harder, L. F. (1990). SPT-based analysis of cyclic pore pressure generation and undrained residual strength. In *Proceedings of the Seed memorial symposium* (ed. J. M. Duncan), pp. 351–376. Vancouver, BC, Canada: BiTech Publishers.

Steedman, R. S., Ledbetter, R. H. & Hynes, M. E. (2000). *The influence of high confining stress on the cyclic behavior of saturated sand*, ASCE Geotechnical Special Publication No. 107, pp. 35–57. Reston, VA, USA: American Society of Civil Engineers.

Stewart, D. P., Chen, Y. R. & Kutter, B. L. (1998). Experience with the use of methylcellulose as a viscous pore fluid in centrifuge models. *Geotech. Testing J.* **21**, No. 4, 365–369.

Vaid, Y. P. & Chern, J. C. (1983). Effect of static shear on resistance to liquefaction. *Soils Found.* **23**, No. 1, 43–60.

Vaid, Y. P. & Chern, J. C. (1985). Cyclic and monotonic undrained response of sands. Advances in the art of testing soils under cyclic loading conditions. *In Advances in the art of testing soils under cyclic conditions* (ed. V. Khosla), pp. 171–176. New York, NY, USA: American Society of Civil Engineers.

Vaid, Y. P. & Finn, W. D. L. (1979). Static shear and liquefaction potential. *J. Geotech. Engng Div., ASCE* **105**, No. GT10, 1233–1246.

Vaid, Y. P., Stedman, J. D. & Sivathayalan, S. (2001). Confining stress and static shear effects in cyclic liquefaction. *Can. Geotech. J.* **38**, No. 3, 580–591.

Whitman, R. V. & Lambe, P. C. (1982). Liquefaction: consequences for a structure. In *Soil dynamics and earthquake engineering: proceedings of the conference on soil dynamics and earthquake engineering* (eds A. S. Cakmak, A. M. Abdel-Ghaffar and C. A. Brebbia), vol. 2, pp. 941–949. Rotterdam, the Netherlands: Balkema.

Yoshimi, Y. & Tokimatsu, K. (1977). Settlement of buildings on saturated sands during earthquakes. *Soils Found.* **17**, No. 1, 23–28.